IEEE Access
Multidisciplinary ⋮ Rapid Review ⋮ Open Access Journal

Received February 11, 2021, accepted March 10, 2021, date of publication March 17, 2021, date of current version March 23, 2021.

Digital Object Identifier 10.1109/ACCESS.2021.3066279

Improving Myoelectric Prosthetic Arm Proportional Control Under MUAP Envelope Colored Noise

SANDRA MARQUEZ-FIGUEROA, (Member, IEEE), YURIY S. SHMALIY, (Fellow, IEEE), AND OSCAR G. IBARRA-MANZANO, (Member, IEEE)
Department of Electronics Engineering, Universidad de Guanajuato, Salamanca 36855, Mexico

Corresponding author: Yuriy S. Shmaliy (shmaliy@ugto.mx)

This work was supported by the Mexican CONACyT-SEP Project under Grant A1-S-10287 and Grant CB2017-2018.

ABSTRACT Accuracy and stability of the myoelectric prosthetic arm digital proportional control strongly depends on shape of the rectified motor unit action potential (MUAP) envelope. To mitigate effects caused by the envelope-induced torque ripples, mechanical vibrations (TRMV), and electromechanical delays (EMD), in this article we develop in discrete-time state-space the unbiased finite impulse response (UFIR) filter, Kalman filter (KF), and game theory recursive H_∞ filter. The filters developed are called the cUFIR filter, cKF, and cH_∞ filter and applied to extract a smooth near Gaussian MUAP envelope by viewing ripples as colored measurement noise (CMN). Additional UFIR and Rauch-Tung-Striebel (RTS) smoothers are also used to improve the performance when the EMD is acceptable. Based on experimental examples of prosthetic arm control, it is shown that the advanced cUFIR filter, cKF, and cH_∞ filter improve the performance of the original filters by the factor of about 10 and essentially reduce the TRMV and EMD.

INDEX TERMS Electromyography, MUAP envelope, filtering, smoothing, prosthetic arm control.

I. INTRODUCTION

The electromyography (EMG) technology has been developed several decades ago [1]–[3] to evaluate and record the electrical activity produced by skeletal muscles [4], [5]. It implies using information extracted along nerves and transmitting informative signals generated by nerves as a series of electrical discharges [6], [7]. In bioengineering, the EMG signals are mostly used to provide efficient control of prostheses, such as artificial arms and feet. To acquire an EMG signal, a needle electrode is inserted through the skin into the muscle and there are recognized several electrical activities. The insertional activity is referred to the electrical activity when a muscle stays at rest. The abnormal spontaneous activity is any neural activity that may occur, for example, due to nerve or muscle damage. Acquired the nerve-generated electrical signals, a motor unit action potential (MUAP) is formed as a sum of all the electrical activities and the MUAP waveform is evaluated to extract useful information about somebody's motion with a sufficient accuracy.

In the standard proportional myoelectric control, a raw MUAP signal goes through a matching amplifier and high-pass filter to a rectifier, which low-pass filter extracts the MUAP envelope. The MUAP envelope is then smoothed, normalized, and converted to a pulse that drives a servo motor or some other device. After normalized, the MUAP envelope can also be digitized using an analog-to-digital converter (ADC) and used as a control signal. In multiple degree of freedom (DOF) control, this scheme is repeated for each DOF and a digitized vector signal is related to a vector control signal via a nonnegative synergy matrix [8]. Although this basic scheme has gained wide currency with various modifications, it has two drawbacks. Smoothing typically causes a biological phenomenon known as the electromechanical delay (EMD), which disrupts a synchronicity between a muscle and a prothesis. Also ''ripples'' in the MUAP envelope cause the torque ripples and mechanical vibrations (TRMV). In some algorithms the EMG data undergo preprocessing to remove the raw EMG data external noise, sensor noise, electrocardiographic interference, spurious background spikes, motion artifacts, and power line interference [7], [9]. As has been shown in [10], [11], extra efforts to clean EMG signals before extracting the envelope generally result in a higher accuracy and stability.

A better and more stable control performance can be achieved in EMG-based digital proportional control. Here,

The associate editor coordinating the review of this manuscript and approving it for publication was Qichun Zhang.

a raw MUAP signal goes through a matching amplifier to an ADC. Then the MUAP bursts are rectified to become positive and the MUAP envelope is extracted using digital signal processing (DSP) methods [4], [6], [7], [12]–[14]. The most widely used standard techniques developed for the MUAP envelope extraction employ the mean square value (MSV) criterion [4], waveform produced by the rectified signal [15], [16], and the Hilbert transform [17]. Since these methods do not completely remove artifacts and ripples, the output is sometimes smoothed that, however, may yield unacceptably large bias errors and does not prevent spikes [18], [19]. The envelope can be improved using the Savitsky-Golay smoother combined with a low-pass filter [20], but only if the time-delay-lag causing EMG is not an issue.

Having a digital EMG signal envelope sequence, more sophisticated methods of optimal and robust filtering are also applied to yield generally a more smooth envelope. The Kalman filter (KF) has been used as an optimal EMG signal envelope extractor in [21]–[26]. Although the KF allows for some improvement with respect to the standard filters, it also incur a significant loss in performance, because ripples in MUAP bursts in no way can be treated as white Gaussian. The performance can be improved using the H_∞ filter, which requires all errors to be just norm bounded. Since ripples in the MUAP burst are bounded by saturation, the game theory H_∞ filter significantly reduces errors by a properly set scalar correction factor θ [27]. However, this filter is highly sensitive to θ and prone to divergence [28]. The unbiased finite impulse response (UFIR) filter [29] is another opportunity to extract a smooth envelope. This filter does not require any information about zero mean noise, is blind on given averaging horizons, and is thus more suitable for EMG signals. Nevertheless, recent investigations have shown [30] that neither of the standard optimal and robust filters is able to make the MUAP envelope near Gaussian. It was suggested in [30] to view ripples in the MUAP envelope as Markov-Gauss colored measurement noise (CMN) and modify the filters [31]–[33]. Even so, the approach still has not been extended to myoelectric control that motivates our present work.

In this article, we design a structure of a digital myoelectric control system for arm proportional control, develop the UFIR, Kalman, and game theory H_∞ filter by viewing ripples in the rectified MUAP signals as CMN, apply these filters along with additional UFIR and Rauch-Tung-Striebel (RTS) smoothers to make the envelope near Gaussian, and test the solutions by experimental examples of myoelectric arm control. The main contributions are the following:

- Structure of a digital myoelectric system for prosthetic arm proportional control.
- Developments of the UFIR, Kalman, and game theory H_∞ filters under CMN for MUAP envelope extraction.
- About tenfold improvement of the myoelectric control performance using the filters developed.

The rest of the article is organized as follows. In Section II, we consider the myoelectric prosthetic arm proportional control problem and formulated the investigation problem. A digital myoelectric proportional control scheme is discussed in Section III. The UFIR, Kalman, and game theory H_∞ filters are developed in Section IV to remove MUAP ripples considered as CMN. Experimental testing of the filters developed is provided in Section V. Applications to prosthetic arm control are given in Section VI and concluding remarks can be found in Section VII.

II. MYOELECTRIC PROSTHETIC ARM PROPORTIONAL CONTROL AND PROBLEM FORMULATION

A sensor array along an arm is used in biotechnology to acquire the EMG signal and nerve studies. It is conducted into sensory action potentials and the compound muscle action potentials. Thereby, an actual arm is used to make control of a prosthetic arm as an intuitive controlling mechanism by using the EMG signal picked up by electrodes. A generative model exploiting surface EMG signals in the context of myoelectric control was proposed in [8], [34]. It assumes that there exists control information at the spinal level, which quantifies the control information as a vector of L force functions

$$F(t) = \left[f^{(1)}(t)\ f^{(2)}(t)\ \dots\ f^{(L)}(t)\right]^T, \tag{1}$$

where $f^{(j)}(t)$, $j \in [1, L]$, is a force function representing the intended activation level of the jth DOF and L is the number of the DOFs. It is also assumed that the activation function vector of M muscles involved in the control is

$$Z(t) = \left[z^{(1)}(t)\ z^{(2)}(t)\ \dots\ z^{(M)}(t)\right]^T \tag{2}$$

where $z^{(i)}(t)$, $i \in [1, M]$, is the ith activation function. Vectors (1) and (2) are coupled with a constant matrix $S \in \mathbb{R}^{M\times L}$ as $Z(t) = SF(t)$, where matrix S indicates that the ith muscle MUAP participates in the activation of the jth prosthesis DOF. Since the jth force function $f^{(j)}(t)$ is a function of a set $Z(t)$ of the activation functions, the ith EMG signal $u^{(i)}(t)$ is linked to the jth force function $f^{(j)}(t)$ by the convolution and it has been emphasized that, due to the dependence $f^{(j)}[t, Z(t)]$, the convolution is a very complex nonlinear transformation. Further substitution of the EMG signal vector

$$U(t) = \left[u^{(1)}(t)\ u^{(2)}(t)\ \dots\ u^{(M)}(t)\right]^T \tag{3}$$

with rectified values provided in the means square value (MSV) sense as

$$\hat{U}^2(t) = \left[\hat{u}^{(1)^2}(t)\ \hat{u}^{(2)^2}(t)\ \dots\ \hat{u}^{(M)^2}(t)\right]^T \tag{4}$$

allows approximating the interaction between $\hat{U}^2(t)$ and $Z(t)$ with a linear matrix form $\hat{U}^2(t) = HZ(t)$, where H is said to be a diagonal matrix $H = \mathrm{diag}(h_1\ h_2\ \dots\ h_M)$ of the gain coefficients h_i, $i \in [1, M]$. That finally results in a relation

$$\hat{U}^2(t) = \tilde{W}F(t), \tag{5}$$

where $\tilde{W} = HS$ couples the force vector $F(t)$ with the EMG vector rectified in the MSV sense as $\hat{U}^2(t)$, and several approaches were developed to implement (5) practically. For example, provided the squared EMG envelope $\hat{U}^2(t)$ for

$M \geqslant L$, the force vector $F(t)$ can be found by solving the inverse linear problem (5) as

$$F(t) = (\tilde{W}^T \tilde{W})^{-1} \tilde{W}^T \hat{U}^2(t)\,. \tag{6}$$

The following drawback of the above approach has be mentioned in [35]. If a user is unable to provide a DOF-wise calibration, then an inadequately determined muscle synergy matrix may result in poor control outcome. An improvement was made in [35] by representing the root MSVs (RMSVs) of an ith MUAP with the T-length signal $\hat{U}(t;T) \in \mathbb{R}^{M\times T}$ and the T-length forced signal vector $F(t;T) \in \mathbb{R}^{2L\times T}$, which are coupled with a latent nonnegative matrix $W \in \mathbb{R}^{M\times 2L}$ as

$$\hat{U}(t;T) = WF(t;T)\,. \tag{7}$$

Referring to the sparseness of the solution, the objective function subject to $W \geqslant 0$ and $F \geqslant 0$ was then chosen as

$$\min_{W,F} \frac{1}{2}\|\hat{U} - WF\|_F^2 + \lambda \sum_{\tau=1}^{T} \|F(t;\tau)\|_1^2\,, \tag{8}$$

where $\|x\|_F$ is the Frobenius norm, $\|x\|_1$ is the 1-norm (or Manhattan norm), and $\lambda > 0$ is a regularization scalar to be optimized. For this classical optimization problem, it was shown that both F and W can be updated iteratively and so that the problem (7) is feasible. Solved (8), the desired force vector F can finally be represented via the myoelectric signal vector similarly to (6).

The approach developed in [35] improves the performance of the approach suggested in [8] by involving signals of length T and solving the optimization problem (8). Nevertheless, it still may be inefficient due to the envelope ripples, which highly affect the control performance. If to reduce ripples by smoothing, then the forced function will experience the EMD, which may disrupt the control synchronicity. The effects can be mitigated if we take into account that the left-hand side in (8) results in the unbiased or maximum likelihood (ML) estimate and the right-hand side can largely be avoided by viewing rippels in the EMG envelope as the colored measurement noise (CMN) that motivates our present work.

The problem now formulates as follows. To improve the myoelectric control performance, we would like to consider and modify a digital myoelectric proportional control scheme, treat ripples in the MUAP signal envelope as CMN, develop the UFIR filter, KF, and game theory H_∞ filter to remove ripples from the MUAP envelope considered as Markov-Gauss CMN, test the solutions by different EMG data, and evaluate the effectiveness for the myoelectric prosthetic arm control.

III. DIGITAL MYOELECTRIC PROPORTIONAL CONTROL SCHEME

A generalized structure of the myoelectric prosthetic arm proportional digital control system considered in this article is shown in Fig. 1. The MUAP signals acquired from M sensors go to the matching amplifier due to low-level amplitudes and the amplified signals are converted by ADCs to digital waveforms. All other operations are provided in digital formats using DSP methods. Namely, digitized data undergo rectification, envelope optimal extraction, and possibly smoothing. The M MUAP envelopes are coupled with L force signals to provide finally control of a prosthesis arm having L DOFs via a constant matrix G determined using the above described approaches [8], [35].

After rectified, M signals $y_k^{(i)}$, $i \in [1, M]$ go to the optimal filter and the envelope of the ith MUAP appears as $s_k^{(i)}$, $i \in [1, M]$. Each MUAP is related to all L or several DOFs and signals $s_k^{(i)}$, $i \in [1, M]$, are coupled with L force signals. The digital vectors of the MUAP envelopes and force functions, respectively,

$$S_k = \left[s_k^{(1)}\ s_k^{(2)}\ \dots\ s_k^{(M)}\right]^T, \tag{9}$$

$$F_k = \left[f_k^{(1)}\ f_k^{(2)}\ \dots\ f_k^{(L)}\right]^T, \tag{10}$$

are coupled via a synergy conversion matrix $G \in \mathbb{R}^{L\times M}$ as

$$F_k = GS_k\,, \tag{11}$$

where matrix G indicates that the ith muscle MUAP participates in the activation of the jth prosthesis DOF. Matrix G can be determined using the techniques developed in [8], [34], [35] and is represented with the relevant matrix in (6). This matrix is commonly supposed to be time-invariant but with an option to be slightly adjusted by a user.

Since the extracted MUAP envelope is typically far from ideal, it can be represents as $S_k = \bar{S}_k + \Delta S_k$, where $\bar{S}_k$ is a desired shape and ΔS_k is a deviation from $\bar{S}_k$. It follows from (11) that in the proportional control, vector F_k will experience an error $\Delta F_k = G\Delta S_k$. To reduce ΔS_k causing TRMV, the Gaussian shape of $\bar{S}_k$ is desirable for two reasons: 1) it does not produce side lobes in the frequency domain and 2) it has smooth edges. Finding a compromise between the MUAP envelope smoothness and EMD is always an issue in myoelectric control as illustrated in Fig. 2, where filtering of the rectified MUAP data is provided by applying an UFIR filter [36] on different averaging horizons of N points, also called time windows. As can be seen, $N = 46$ allows for a well-smoothed first burst, while the more intensive second one is not well shaped. By $N = 180$, the second burst acquire an acceptable shape and the first one becomes more smooth. However, latency in both envelopes may cause an unacceptable EMD and errors in the force function calculation. In what follows, we will show that improving the force function shape, thereby avoiding essential TRMV and EMD, can be provided by viewing ripples in the MUAP envelope as CMN.

A. STATE-SPACE MODEL OF MUAP ENVELOPE

Looking into signals in Fig. 1, one can resume that $y_k^{(i)}$ is highly noisy and thus cannot be involved directly to myoelectric control. Furthermore, noise is not white Gaussian and hence optimal estimators such as the KF will not serve

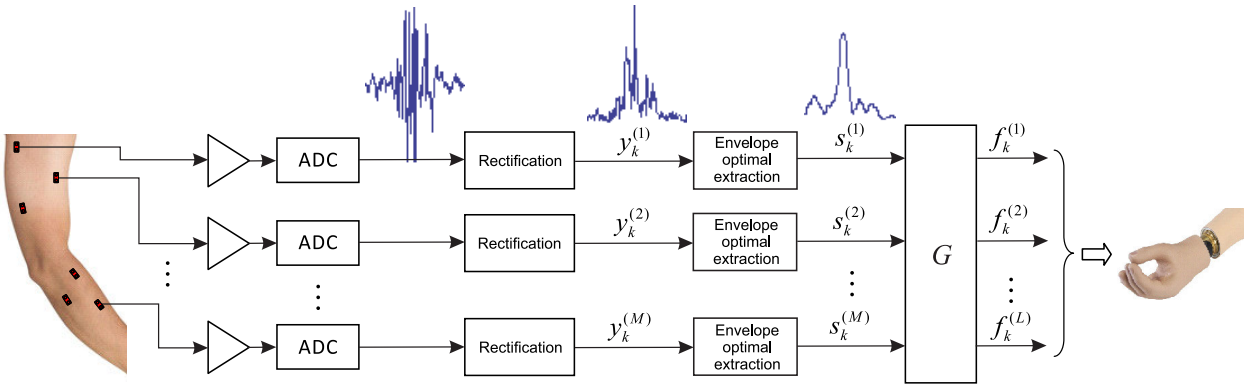

FIGURE 1. A generalized structure of the myoelectric prosthetic arm direct proportional digital control system.

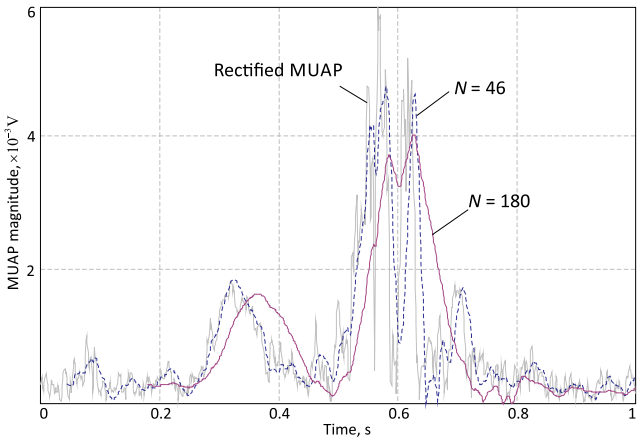

FIGURE 2. Extracting the envelope from a rectified MUAP signal by applying an UFIR filter on different horizons.

properly. On the other hand, variations in the rectified MUAP (Fig. 2) are reminiscent of a strongly colored Markov-Gauss noise [33], although having another physical meaning. Since a desirable envelope is Gaussian, we approximate it between two discrete points with a degree polynomial, introduce a state $x_k^{(i)} \in \mathbb{R}^K$, where K is the number of the MUAP envelope states, and represent with the following state space model

$$x_k^{(i)} = Ax_{k-1}^{(i)} + Bw_k^{(i)}, \tag{12}$$

$$y_k^{(i)} = Hx_k^{(i)} + v_k^{(i)}, \tag{13}$$

where $y_k^{(i)}$ is a scalar observation of the ith MUAP envelope. For polynomial approximation, entries of matrix $A \in \mathbb{R}^{K\times K}$ are defined by the Taylor series [37],

$$A = \begin{bmatrix} 1 & \tau & \frac{\tau^2}{2} & \dots & \frac{\tau^{K-1}}{(K-1)!} \\ 0 & 1 & \tau & \dots & \frac{\tau^{K-2}}{(K-2)!} \\ 0 & 0 & 1 & \dots & \frac{\tau^{K-3}}{(K-3)!} \\ \vdots & \vdots & \vdots & \ddots & \vdots \\ 0 & 0 & 0 & \dots & 1 \end{bmatrix}. \tag{14}$$

The envelope zero mean noise $w_k^{(i)} \in \mathbb{R}^P$ is still a subject for deep investigations along with a proper matrix $B \in \mathbb{R}^{K\times P}$ and the observation matrix is $H = [1\,0\dots0] \in \mathbb{R}^{1\times K}$. In the first order approximation, $w_k^{(i)}$ can be supposed to be white Gaussian, $w_k^{(i)} \sim \mathcal{N}(0, Q^{(i)})$, with the covariance $Q^{(i)}$. But most realistically it can be viewed as colored or even as a bounded disturbance. Finally, the scalar measurement error $v_k^{(i)}$ representing variations and artifacts in the MUAP envelope in no way can be treated as white Gaussian. Looking into Fig. 2, $v_k^{(i)}$ can be thought of as CMN and, as suggested in [30], we represent it with the Markov-Gauss model

$$v_k^{(i)} = \psi^{(i)} v_{k-1}^{(i)} + \xi_k^{(i)}, \tag{15}$$

where $0 < \psi^{(i)} < 1$ is a coloredness factor associated with the ith MUAP. A scalar zero mean driving noise $\xi_k^{(i)}$ is still also a subject for investigations. In this article, we will suppose that this noise is white Gaussian, $\xi_k^{(i)} \sim \mathcal{N}(0, \sigma_\xi^{(i)^2})$, with the standard deviation $\sigma_\xi^{(i)}$, although it can also be thought of as having a uniform or even heavy-tailed distribution.

Estimated the rectified MUAP envelope state vector by (28) as $\hat{x}_k^{(i)}$, the envelope signal $s_k^{(i)}$ can be calculated as $s_k^{(i)} = \hat{x}_{1k}^{(i)}$, where $\hat{x}_{1k}^{(i)}$ is the first state in vector $\hat{x}_k^{(i)}$, and vectors (9) and (10) coupled with one another by $F_k = GS_k$ (11) as

$$\begin{bmatrix} f_k^{(1)} \\ f_k^{(2)} \\ \vdots \\ f_k^{(l)} \end{bmatrix} = \begin{bmatrix} g_{11} & g_{12} & \dots & g_{1M} \\ g_{21} & g_{22} & \dots & g_{2M} \\ \vdots & \vdots & \ddots & \vdots \\ g_{L1} & g_{L2} & \dots & g_{LM} \end{bmatrix} \begin{bmatrix} s_k^{(1)} \\ s_k^{(2)} \\ \vdots \\ s_k^{(M)} \end{bmatrix}, \tag{16}$$

where the components of matrix G can be specified by (6) or solving (8) using the approaches developed in [8], [35].

IV. ALGORITHM FOR MUAP ENVELOPE EXTRACTION UNDER CMN

To apply filtering algorithm for model (12) and (13) with CMN (15), we use the approach originally proposed in [31] and developed in [30], [33]. To this end, we first transform the observation model to another one with white Gaussian noise and then modify the filtering algorithms.

A. STATE SPACE MODEL TRANSFORMATION

To avoid the CMN $v_k^{(i)}$ in (13), consider a new observation $\zeta_k^{(i)}$ as measurement differences and write

$$\begin{aligned}\zeta_k^{(i)} &= y_k^{(i)} - \psi^{(i)} y_{k-1}^{(i)}\,,\\ &= Hx_k^{(i)} + v_k^{(i)} - \psi^{(i)} Hx_{k-1}^{(i)} - \psi^{(i)} v_{k-1}^{(i)}\,.\end{aligned} \tag{17}$$

Then represent (16) in the standard form as

$$\zeta_k^{(i)} = D^{(i)} x_k^{(i)} + \bar{v}_k^{(i)}\,, \tag{18}$$

where $D^{(i)} = H - \Gamma^{(i)}$, $\Gamma^{(i)} = \psi^{(i)} HF^{-1}$, and the scalar white Gaussian noise $\bar{v}_k^{(i)} \sim \mathcal{N}(0, \sigma_{\bar{v}}^{(i)^2})$ is

$$\bar{v}_k^{(i)} = \Gamma^{(i)} B w_k^{(i)} + \xi_k^{(i)} \tag{19}$$

with the properties

$$\sigma_{\bar{v}}^{(i)^2} = E\{\bar{v}_k^{(i)^2}\} = \Gamma^{(i)}\Phi^{(i)} + \sigma_{\xi}^{(i)^2}\,, \tag{20}$$

$$L^{(i)} = E\{\bar{v}_k^{(i)} w_k^{(i)^T}\} = \Gamma^{(i)} B Q^{(i)}\,, \tag{21}$$

where matrix $\Phi^{(i)}$ is defined by

$$\Phi^{(i)} = BQ^{(i)} B^T \Gamma^{(i)^T}\,. \tag{22}$$

We can now work with a new state-space model (12) and (18), in which $w_k^{(i)}$ and $\bar{v}_k^{(i)}$ are white Gaussian, but time-correlated with the covariance $L^{(i)}$ given by (20). Provided (12) and (18), the UFIR filter, KF, and H_∞ filter can be modified as will be shown next.

B. UFIR FILTERING ALGORITHM

The iterative UFIR filtering algorithm [37], [38] employs most recent data from a horizon $[m, k]$ of N points, where $m = k - N + 1$, and does not require any information about zero mean noise and initial values. This filter is thus most suitable for the MUAP envelope extraction, provided that the horizon is set optimally in the MSE sense as N_{opt}. Now observe that $w_k^{(i)}$ and $\bar{v}_k^{(i)}$ are both white and zero mean and that their time-correlation does not yield any bias. Thus, the UFIR filter can be applied directly to (12) and (17) as shown in [36] if we modify matrices. To recognize the difference, we will call the UFIR filter modified for CMN the cUFIR filter.

The cUFIR filter can be designed for the ith MUAP envelope as follows. Given the horizon length N, rectified MUAP data $y_k^{(i)}$, and proper $\psi^{(i)}$, the initial state can be computed in a short batch form as [36]

$$\bar{x}_s^{(i)} = \mathcal{G}_s^{(i)} C_{m,s}^{(i)^T} Y_{m,s}^{(i)} \tag{23}$$

using the extended data vector

$$Y_{m,s}^{(i)} = \begin{bmatrix} y_m^{(i)} & y_{m+1}^{(i)} & \cdots & y_k^{(i)} \end{bmatrix}^T \tag{24}$$

and the generalized noise power gain (GNPG) $\mathcal{G}_s^{(i)} = (C_{m,s}^{(i)^T} C_{m,s}^{(i)})^{-1}$, where a short batch matrix $C_{m,s}^{(i)}$ is composed of matrices A and $D^{(i)}$ as

$$C_{m,s}^{(i)} = \begin{bmatrix} D^{(i)} A^{-(K-1)} \\ \vdots \\ D^{(i)} A^{-1} \\ D^{(i)} \end{bmatrix}. \tag{25}$$

Then both $\bar{x}_s^{(i)}$ and $\mathcal{G}_s^{(i)}$ can be updated iteratively using an auxiliary time index l starting with $l = s + 1$ and using the recursions

$$\zeta_l^{(i)} = y_l^{(i)} - \psi^{(i)} y_{l-1}^{(i)}\,, \tag{26}$$

$$D^{(i)} = H - \psi^{(i)} HA^{-1}\,, \tag{27}$$

$$\mathcal{G}_l^{(i)} = [D^{(i)^T} D^{(i)} + (A\mathcal{G}_{l-1}^{(i)} A^T)^{-1}]^{-1}\,, \tag{28}$$

$$K_l^{(i)} = \mathcal{G}_l^{(i)} D^{(i)^T}\,, \tag{29}$$

$$\bar{x}_l^{(i)} = A\bar{x}_{l-1}^{(i)} + K_l^{(i)}(\zeta_l^{(i)} - D^{(i)} A\bar{x}_{l-1}^{(i)})\,, \tag{30}$$

and the output estimate is taken when $l = k$ as $\hat{x}_k^{(i)} = \bar{x}_k^{(i)}$. It can easily be shown that $\psi^{(i)} = 0$ makes the cUFIR filter the standard UFIR filter.

The error covariance $P_k^{(i)}$ of the UFIR filter can be computed approximately by the KF error covariance if to replace the Kalman gain K_k with $\mathcal{G}_k D^{(i)^T}$ as

$$\begin{aligned}P_k^{(i)} &= (I - \mathcal{G}_k^{(i)} D^{(i)^T} D^{(i)}) P_k^{(i)-} (I - \mathcal{G}_n D^{(i)^T} D^{(i)})^T\\ &\quad + \mathcal{G}_k^{(i)} D^{(i)^T} (\Gamma^{(i)}\Phi^{(i)} + R) D^{(i)} \mathcal{G}_k^{(i)}\\ &\quad - 2(I - \mathcal{G}_k^{(i)} D^{(i)^T} D^{(i)}) \Phi^{(i)} D^{(i)} \mathcal{G}_k^{(i)}\\ &= P_k^{(i)-} - 2(P_k^{(i)-} D^{(i)^T} + \Phi^{(i)}) D^{(i)} \mathcal{G}_k^{(i)}\\ &\quad + \mathcal{G}_k^{(i)} D^{(i)^T} \mathcal{S}_n^{(i)} D^{(i)} \mathcal{G}_k^{(i)}\\ &= P_k^{(i)-} - (2P_k^{(i)-} D^{(i)^T} + 2\Phi^{(i)}\\ &\quad + \mathcal{G}_k^{(i)} D^{(i)^T} \mathcal{S}_k^{(i)}) D^{(i)} \mathcal{G}_k^{(i)}\,,\end{aligned} \tag{31}$$

where the prior error covariance $P_k^{(i)}$ and innovation covariance $\mathcal{S}_k^{(i)}$ are given by

$$P_k^{(i)-} = AP_{k-1}^{(i)} A^T + BQ^{(i)} B^T\,, \tag{32}$$

$$\begin{aligned}\mathcal{S}_k^{(i)} &= D^{(i)} P_k^{(i)-} D^{(i)^T} + R\\ &\quad + H\Phi^{(i)} + \Phi^{(i)^T} D^{(i)^T}\,.\end{aligned} \tag{33}$$

Although the cUFIR algorithm does not require the error covariance, unlike the KF, matrix $P_k^{(i)}$ may be needed to evaluate filtering errors.

C. KALMAN FILTERING ALGORITHM

The KF can be developed as cKF to extract the ith MUAP envelope under CMN as follows. Given the initial $\hat{x}_0^{(i)}$ and $P_0^{(i)}$ and the coloredness factor $\psi^{(i)}$, the prior error covariance is computed by

$$P_k^{(i)-} = AP_{k-1}^{(i)} A^T + Q^{(i)}\,. \tag{34}$$

The estimate and error covariance can then be updated by developing the alternative KF recursions originally derived

in [27] and modified in [28]. Accordingly, we have

$$\zeta_k^{(i)} = y_k^{(i)} - \psi^{(i)} y_{k-1}^{(i)}, \tag{35}$$
$$D^{(i)} = H - \psi^{(i)} H A^{-1}, \tag{36}$$
$$\Gamma^{(i)} = \psi^{(i)} H A^{-1}, \tag{37}$$
$$\bar{R}^{(i)} = \sigma_{\tilde{v}}^{(i)^2} = \Gamma^{(i)} B Q^{(i)} B^T \Gamma^{(i)^T} + \sigma_{\xi}^{(i)^2}, \tag{38}$$
$$P_k^{(i)} = P_k^{(i)-} (I + D^{(i)^T} \bar{R}^{(i)^{-1}} \bar{D}^{(i)} P_k^{(i)-})^{-1}, \tag{39}$$
$$K_k^{(i)\mathrm{K}} = P_k^{(i)} D^{(i)^T} \bar{R}^{(i)^{-1}}, \tag{40}$$
$$\hat{x}_k^{(i)} = A\hat{x}_{k-1}^{(i)} + K_k^{(i)\mathrm{K}} (\zeta_k^{(i)} - D^{(i)} A \hat{x}_{k-1}^{(i)}), \tag{41}$$
$$P_{k+1}^{(i)-} = A P_k^{(i)} A^T + Q^{(i)}. \tag{42}$$

As can be seen, the coloredness factor $\psi^{(i)}$ has a more strong effect on the KF estimate (41) via matrices $D^{(i)}$ and $\bar{R}^{(i)}$, while the UFIR estimate is affected by $\psi^{(i)}$ only via $D^{(i)}$.

D. RECURSIVE H_∞ FILTERING ALGORITHM

The game theory recursive H_∞ filter originally derived in [27] can be developed for the ith MUAP envelope under CMN as cH_∞ similarly to the KF. Given the initial $\hat{x}_0^{(i)}$ and $P_0^{(i)}$ and the coloredness factor $\psi^{(i)}$, the prior error covariance $\check{P}^{(i)-}$ can be computed by (34) and the vectors and matrices updated using the following recursive forms,

$$\zeta_k^{(i)} = y_k^{(i)} - \psi^{(i)} y_{k-1}^{(i)}, \tag{43}$$
$$D^{(i)} = H - \psi^{(i)} H A^{-1}, \tag{44}$$
$$\Gamma^{(i)} = \psi^{(i)} H A^{-1}, \tag{45}$$
$$\check{\bar{R}}^{(i)} = \Gamma^{(i)} B Q^{(i)} B^T \Gamma^{(i)^T} + \check{R}^{(i)}, \tag{46}$$
$$\check{P}_k^{(i)} = \check{P}_k^{(i)-} (I - \theta^{(i)} S^{(i)} \check{P}_n^{-} + D^{(i)^T} \check{\bar{R}}^{(i)^{-1}} \bar{D}^{(i)} \check{P}_k^{(i)-})^{-1}, \tag{47}$$
$$K_k^{(i)\infty} = \check{P}_k^{(i)} D^{(i)^T} \check{\bar{R}}^{(i)^{-1}}, \tag{48}$$
$$\hat{x}_k^{(i)} = A\hat{x}_{k-1}^{(i)} + K_k^{(i)\infty} (\zeta_k^{(i)} - D^{(i)} A \hat{x}_{k-1}^{(i)}), \tag{49}$$
$$\check{P}_{k+1}^{(i)-} = A \check{P}_k^{(i)} A^T + \check{Q}^{(i)}, \tag{50}$$

where $\check{R}^{(i)}$ is the measurement error variance corresponding to $\sigma_{\xi}^{(i)^2}$ in the KF. Note that the user-chosen symmetric positive definite error matrices $\check{P}_0^{(i)}$, $\check{Q}^{(i)}$, and $\check{R}^{(i)}$ have another meaning than in the KF. To guarantee the H_∞ filter stability, a positive definite matrix $S^{(i)}$ is subjected to the constraint

$$(\check{P}_k^{(i)-})^{-1} - \theta^{(i)} S^{(i)} + D^{(i)^T} \check{R}^{(i)^{-1}} D^{(i)} > 0. \tag{51}$$

If all errors are required to be weighted equally, then matrix $S^{(i)}$ can be assigned to be identity, $S^{(i)} = I$, and we notice that a better performance is obtained by a small enough positive scalar $\theta^{(i)} > 0$. It worth noting that, by $\theta^{(i)} = 0$, the H_∞ filter becomes the KF. However, care must be taken to set $\theta^{(i)}$ properly to avoid the divergence [28], [29].

V. EXPERIMENTAL TESTING

In this section we apply the cUFIR, cKF, and cH_∞ algorithms designed to extract smooth envelopes from various biosignals acquired from muscles as caused by user motions. As benchmarks, all along we will employ the standard UFIR, KF, and H_∞ algorithms. First, we will analyse the EMG signals to infer if they have any indications, signs, symptoms, diagnosis or treatment of any disease, disorder, or abnormality, for which the Hilbert transform is required to shape the envelope. Next, we will identify the EMG signal features. For the ith rectified MUAP, we will specify model (12)–(13) with two states, $K = 2$, and matrices

$$A = \begin{bmatrix} 1 & \tau \\ 0 & 1 \end{bmatrix}, \quad B = \begin{bmatrix} \frac{\tau^2}{2} \\ \tau \end{bmatrix}, \quad H = \begin{bmatrix} 1 & 0 \end{bmatrix}.$$

We suppose that the envelope noise $w_k^{(i)} \sim \mathcal{N}(0, \sigma_w^{(i)^2})$ acts in the third state and is projected to state $x_k^{(i)}$ by matrix B. Noise $v_k^{(i)}$ is supposed to be Markov-Gauss (15) with the coloredness factor $\psi^{(i)}$, which will be measured experimentally to provide the most smooth envelope with a minimum latency.

The filters will be applied to EMG signal databases "S1_A1_E1", "S1_A1_E2", and "S1_A1_E3" publicly available from [39]–[41]. These signals are generated by male's right hand, 31 years old and stood 1.70 meters tall: "S1_A1_E1" represents a basic movements of the fingers, "S1_A1_E2" isometric, isotonic hand configurations, and basic wrist movements, and "S1_A1_E3" grasping and functional movements. We start with the NinaPro database [41], which contains kinematic and EMG data taken from the upper limbs of 27 intact subjects while performing 52 finger, hand, and wrist movements of interest.

A. MOTION RECOGNITION IN EMG DATA

The enrolled database includes 27 intact subjects of 20 men and 7 women aged between 22–40 years (28.6 ± 4.2 years as the mean age) with three different exercises previously diagnosed by a professional. All data are collected using the Cyberglove 2 data glove and the 10x Otto Bock MyoBock (electrodes). Each subject performs three exercises:

- Basic movements of fingers.
- Isometric, isotonic hand configurations in basic wrist movements.
- Grasping and functional movements.

1) FIRST MOTION

The EMG signals described in [40], [42] are acquired using 10 Otto Bock MyoBock 13E200 electrodes, while kinematic data are acquired using a Cyberglove 2 data. The database includes 52 different movements, each of which was repeated 10 times by each subject.

We begin with a surface EMG signal collected from the basic movements of the fingers made by a 28-year-old man [41]. In Fig. 3a we shows the rectified raw EMG signal shaped using the Hilbert transform. In Fig. 3a we give the envelopes extracted using the standard UFIR, Kalman, and H_∞ filters and Fig. 2c sketches the envelopes obtained by the cUFIR filter, cKF, and cH_∞ filter modified for CMN.

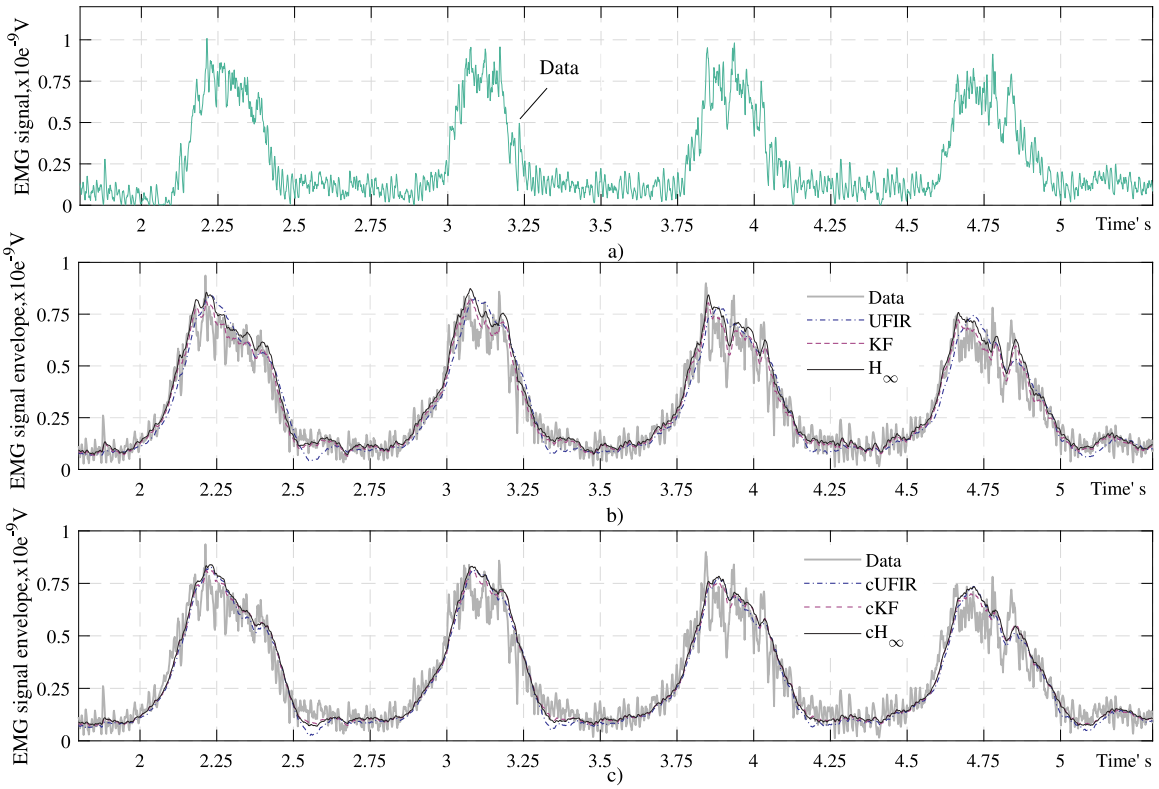

FIGURE 3. EMG signal (1.75…5.25)ms available from [41]: (a) rectified EMG signal obtained using the Hilbert transform, (b) envelopes extracted using standard UFIR filter, KF, and H_∞ filter, and (c) envelopes extracted using cUFIR filter, cKF, and cH_∞ filter.

The results were obtained inder the ideal conditions when all estimators are tuned properly with $N_{\text{opt}} = 140$, $\sigma_\xi = 50\,\mu\text{V}$, $\sigma_w = 0.1\,\text{V/s}^2$, $S_n = I$, $\psi = 0.65$, and $\theta = 10^{-6}$.

What can be seen is that the envelopes extracted by the modified filters are more smooth than by the standard filters and that there is non visible latency in the estimates. The filters produce consistent estimates, although the UFIR and cUFIR filters perform better.

2) SECOND MOTION

We next consider an EMG signal generated by grasping and functional movements of a 31 year old man [41]. The selected part of the rectified MUAP is shown in Fig. 4a and the relevant envelopes extracted by the standard and modified filters in Fig. 4b and Fig. 4c, respectively, for $\psi_{\text{opt}} = 0.65$. Again we see that ripples are much lesser intensive in the envelopes extracted using the modified filters and that the UFIR filter performs better than others.

3) THIRD MOTION

Quite another MUAP bursts having sharp edges can be observed in the third motion shown in Fig.5a. The Hilbert transform inherently erodes sharp edges as shown in Fig.5b and Fig.5c that allows for extracting more smooth envelopes. Again we see that the modified filters are more successful in smoothing the envelope and that the standard UFIR filter performs better than the KF and H_∞ filter.

What can be concludes now is that the Gauss-Markov interpretation of variations in the MUAP envelope makes it possible to extract acceptably smooth envelopes. It should also be pointed out that the colorodness factor ψ 1) must be optimized to provide the best envelope shaping and 2) should not exceed 1.0 to satisfy the requirements of the CMN stationarity.

B. FURTHER SMOOTHING MUAP ENVELOPE

We now conduct additional investigations aimed at further smoothing of the MUAP envelopes and their dips and peaks. For this purpose, we apply two smoothers to the previously extracted envelopes shown in Fig. 3–Fig. 5: the p-shift batch UFIR filter operating in the smoother mode with a lag $q = -p$ [36] and depicted as UFIRs and the RTS smoother [43]. The results of the additional smoothing sketched in Fig. 6 for $N_{\text{opt}} = 140$ and $q = 10$ allow arriving at the following inferences. Setting a short lag q of several discrete points allows for a better smoothing of the envelope ripples while not introducing an essential time delay. It is also seen that the UFIR smoother fulfils this job better.

C. THE GAUSSIAN TEST

The MUAP Gaussian envelope is most desirable for myoelectric control due to the following important features: 1) smooth edges in the time domain and 2) no side lobes in the frequency domain. This requirement is supported by the observation that the power spectrum of a single motor unit

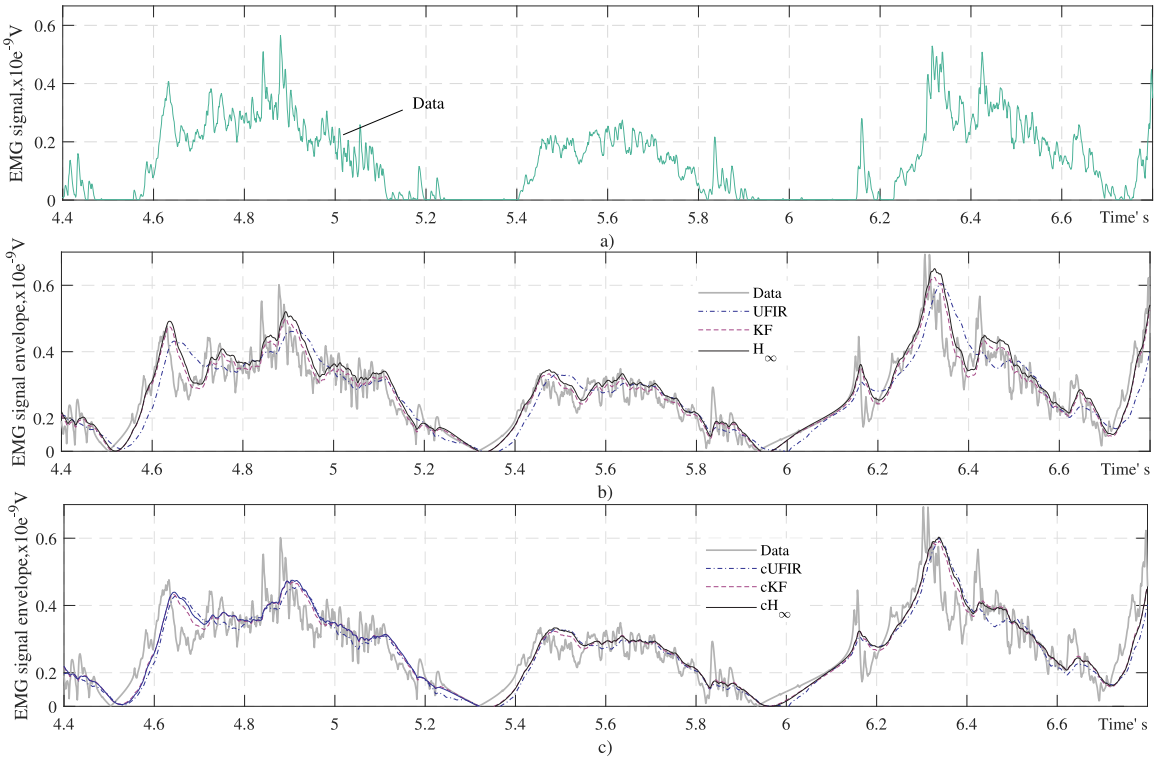

FIGURE 4. EMG signal (6.2…8.6)s available from [41]: a) Rectified MUAP obtained using the Hilbert transform, b) envelopes extracted by the UFIR filter, KF, and H_∞ filter, and c) envelopes extracted by the cUFIR filter, cKF, and cH_∞ filter.

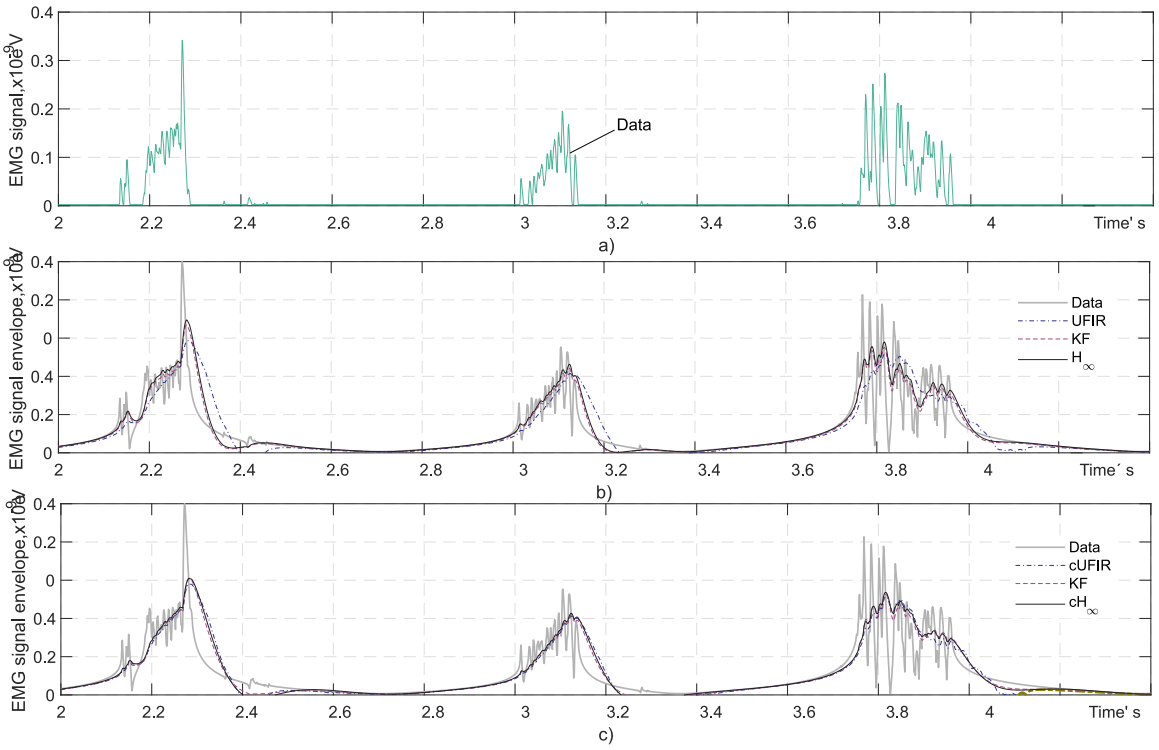

FIGURE 5. EMG signal (4.5…6.7)s available from [41]: a) rectified MUAP shaped using the Hilbert transform, b) envelopes extracted by the UFIR filter, KF, and H_∞ filter, and c) envelopes extracted by the cUFIR filter, cKF, and cH_∞ filter.

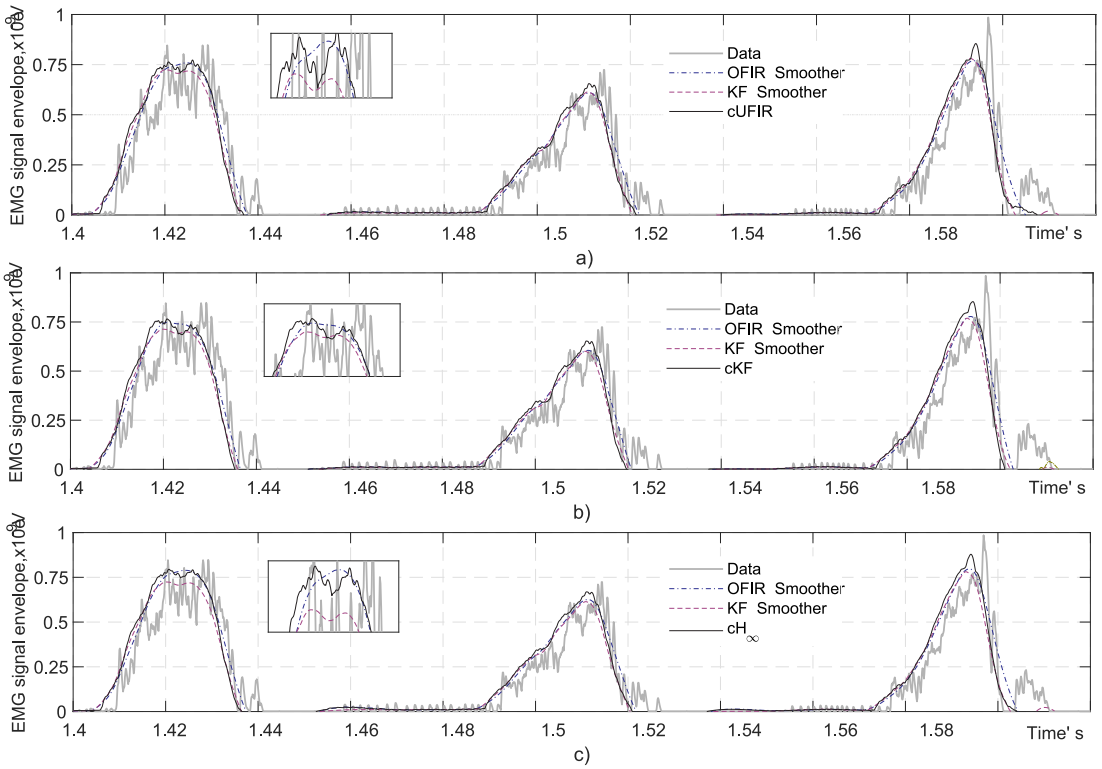

FIGURE 6. Additionally smoothed MUAP envelopes (1.4…1.6)s available from [41] and zoomed peaks.

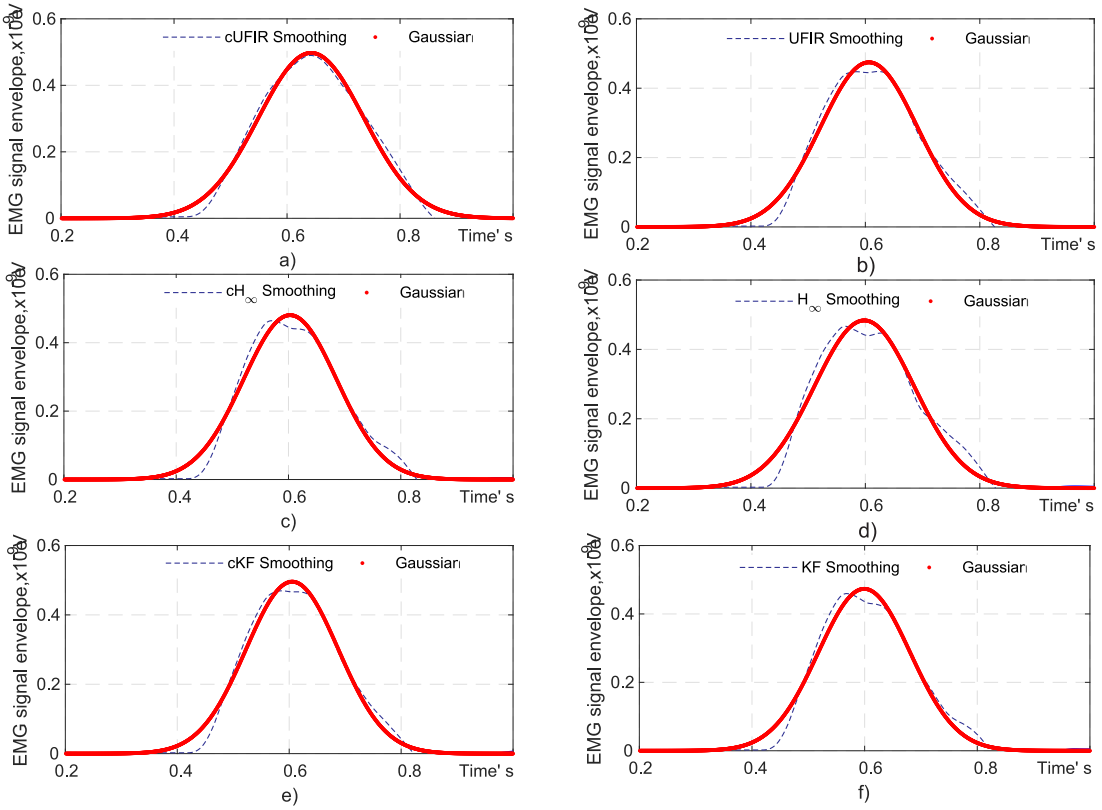

FIGURE 7. Testing by the Gaussian pulse in the MSE sense the MUAP envelopes extracted using the following smoothers: (a) cUFIR, (b) UFIR, (c) cH_∞, d) H_∞, (e) RTS, and (f) cRTS.

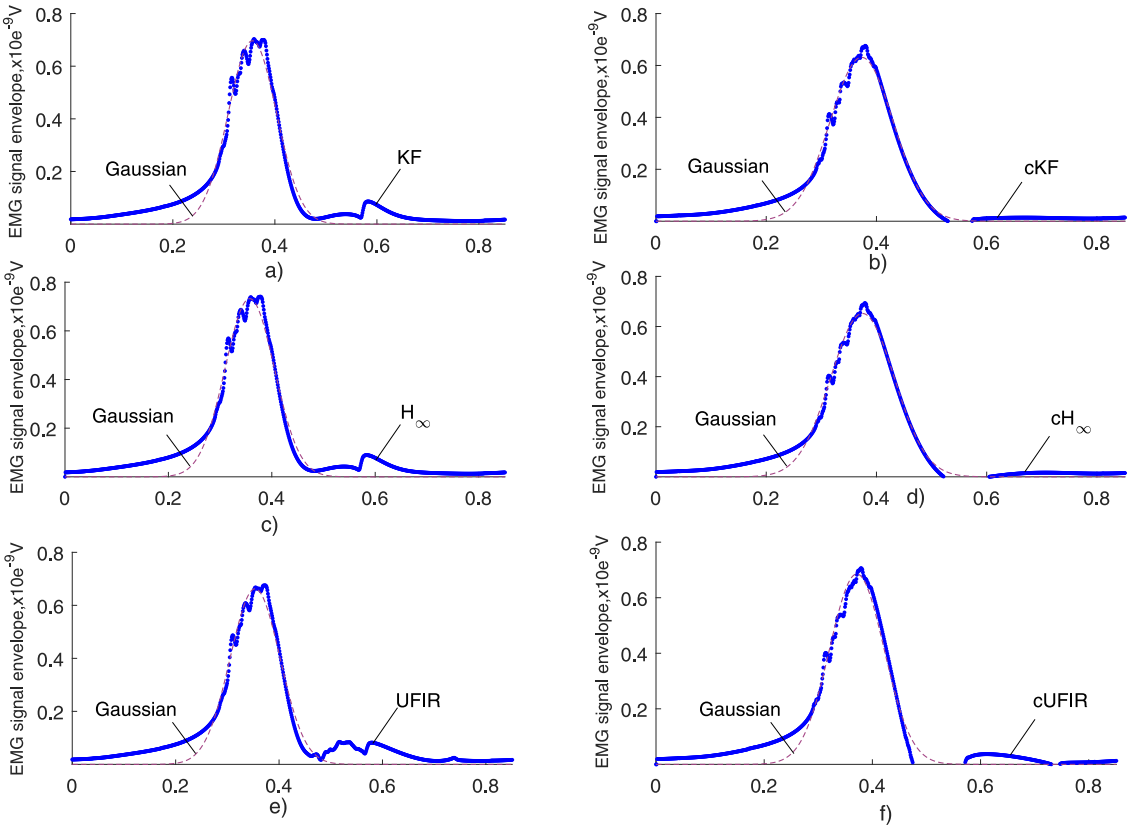

FIGURE 8. Testing MUAP rippled envelopes extracted by the estimators for Gaussianity in the MSE sense: (a) cUFIR, (b) UFIR, (c) cH_∞, (d) H_∞, (e) cKF, and (f) KF.

TABLE 1. Testing extracted MUAP envelopes for Gaussianity.

Filter	RMSE		
	"S14_A1_E3"	"S1_A1_E2"	"S1_A1_E1"
KF	0.04057	0.1011	0.09841
H_∞	0.04249	0.1043	0.1014
UFIR	0.04319	0.09264	0.09345
cKF	0.02751	0.07254	0.07752
cH_∞	0.02903	0.07482	0.0797
cUFIR	0.04421	0.08862	0.08451

TABLE 2. Testing extracted MUAP envelopes with ripples for Gaussianity.

	RMSE		
	Filter	Filter/UFIRs	Filter/RTS
KF	0.03149	0.02684	0.02413
UFIR	0.0313	0.02199	0.02388
H_∞	0.04068	0.022463	0.02906
cKF	0.0276	0.0198	0.02109
cUFIR	0.02623	0.01968	0.0212
cH_∞	0.02885	0.02184	0.02214

firing with a mean rate of 15 spikes per second has a Gaussian envelope [44]–[46]. One may thus suppose that the Gaussian shape is inherent to the MUAP envelope, where the parameters of interest are time, duration, and amplitude of the activity phases. Even so, the Gaussian shape is not the only one associated with the MUAP envelope applications [47], [48].

In Fig. 7, the Gaussian pulse is positioned to provide the best approximation in the MSE sense of the extracted MUAP envelope in the "S1_A1_E1" signal and table 1 lists the root MSEs (RMSEs) produced by different estimators for the Gaussian pulse. What can be concluded is that the modified filters (cKF, cH_∞, and cUFIR) are more successful in approaching the Gaussian pulse than the original filters (KF, H_∞, and UFIR).

Another test for Gaussianity has been applied to the extracted MUAP envelopes, which demonstrate ripples as shown in Fig.8. The envelopes were obtained using filters and additional smoothers as described above and we notice that N_{opt} has appeared to be a bit larger than in the previous case. Table 2 supports the results with numerically computed RMSEs obtained with respect to the Gaussian pulse. As can be seen, an additional smoothing improves the envelope shape and makes it such that all outputs become quite acceptable for myoelectric control.

VI. APPLICATIONS TO PROSTHETIC ARM CONTROL

We finally consider an example of applications to prosthetic arm control. We use muscular contractions of the wrist and basic movements of the fingers to provide the system control. The initial conditions are forced to zero in order to implement

the positions of the joints given by the trajectories obtained from the EMG envelope. Since such an organization admits sudden speed changes, the joint angle variations can be high between two neighboring time instances. As a benchmark, we used the PD control with values $k_v > 0$ and $K_p > 0$, where k_v is the differential constant and K_p is the proportionality constant. The PD controller was implemented for the specified time to find the RMSE and thus obtain a cost function to provide a better fit.

In Table 3, we list the minimum wrist joint angular RMSEs accumulated in a specific time from an initial position to the desired position for each estimate. The estimates are provided by filters (Filter) and filters with additional smoothers (Filter/UFIRs and Filter/RTS). The original rectified MUAP (no filtering is applied) produces an angular error of 0.0012 rad. The application of the original UFIR, Kalman, and H_∞ filters improves the performance by the factor of about 10-15 and further improvement by the factor of about 10 is achieved using the developed cUFIR filter, cKF, and cH_∞ filters. This example neatly demonstrates that treating the MUAP envelope ripples as CMN allows getting a much bigger progress in the design of prosthetic arm control systems.

TABLE 3. Error of the motor in a specific time.

	Wrist joint RMSE, rad		
	Filter	Filter/UFIRs	Filter/RTS
KF	4.0235e-05	3.3435e-05	3.4984e-05
H_∞	1.1658e-04	6.3637e-05	7.2696e-05
UFIR	8.9823e-05	6.3579e-05	6.7267e-05
cKF	7.9732e-06	5.1927e-06	5.5652e-06
cH_∞	8.2010e-06	5.8703e-06	6.1774e-06
cUFIR	7.3807e-06	5.1927e-06	5.5652e-06

VII. CONCLUSIONS

The cUFIR filter, cKF, and game theory recursive cH_∞ filtering algorithms developed in this article for rectified MUAP signals assuming CMN in the envelope have demonstrated a dramatic improvement by the factor of about 10 in the MUAP smooth envelope extraction. The effect has been achieved by suppressing the colored noise-like ripples and other variations in the MUAP envelope with no essential time delays. It was also demonstrated that the Gaussian-like smooth envelope can be extracted from the rectified MUAP signal avoiding fast variations and EMD in the force function.

Using the filters developed in the digital myoelectric prosthetic arm proportional control systems allows getting a more reliable and stable effect. Based upon extensive investigations, we suggest using the cKF if proper tuning is feasible under ripples in the rectified MUAP signal. The cH_∞ filter may improve the cKF performance, but it may also diverge if the tuning factor is set incorrectly. Otherwise, the cUFIR filter, which ignores zero mean noise and is thus more robust, can be a better choice. Additional smoothing by the UFIR and RTS smoothers improves the MUAP envelope Gaussianity. However, it also increases the bias errors and so that a care must be taken to avoid large EMD in practical designs.

REFERENCES

[1] J. G. Kreifeldt, "Signal versus noise characteristics of filtered EMG used as a control source," *IEEE Trans. Biomed. Eng.*, vol. BME-18, no. 1, pp. 16–22, Jan. 1971.

[2] E. N. Kamavuako, K. B. Englehart, W. Jensen, and D. Farina, "Simultaneous and proportional force estimation in multiple degrees of freedom from intramuscular EMG," *IEEE Trans. Biomed. Eng.*, vol. 59, no. 7, pp. 1804–1807, Jul. 2012.

[3] X. Zhang, D. Wang, Z. Yu, X. Chen, S. Li, and P. Zhou, "EMG-torque relation in chronic stroke: A novel EMG complexity representation with a linear electrode array," *IEEE J. Biomed. Health Inform.*, vol. 21, no. 6, pp. 1562–1572, Nov. 2017.

[4] T. D'Alessio and S. Conforto, "Extraction of the envelope from surface EMG signals," *IEEE Eng. Med. Biol. Mag.*, vol. 20, no. 6, pp. 55–61, Nov./Dec. 2001.

[5] J. Shi, Z. Yong-Ping, H. Qing-Hua, and X. Chen, "Continuous monitoring of sonomyography, electromyography and torque generated by normal upper arm muscles during isometric contraction: Sonomyography assessment for arm muscles," *IEEE Trans. Biomed. Eng.*, vol. 55, no. 3, pp. 1191–1198, Mar. 2008.

[6] A. Merlo, D. Farina, and R. Merletti, "A fast and reliable technique for muscle activity detection from surface EMG signals," *IEEE Trans. Biomed. Eng.*, vol. 50, no. 3, pp. 316–323, Mar. 2003.

[7] M. Reaz, M. Hussain, and F. Mohd-Yasin, "Techniques of EMG signal analysis: Detection, processing, classification and applications (correction)," *Biol. Procedures Online*, vol. 8, no. 1, p. 163, 2006.

[8] N. Jiang, K. B. Englehart, and P. A. Parker, "Extracting simultaneous and proportional neural control information for multiple-DOF prostheses from the surface electromyographic signal," *IEEE Trans. Biomed. Eng.*, vol. 56, no. 4, pp. 1070–1080, Apr. 2009.

[9] S. Thongpanja, A. Phinyomark, F. Quaine, Y. Laurillau, C. Limsakul, and P. Phukpattaranont, "Probability density functions of stationary surface EMG signals in noisy environments," *IEEE Trans. Instrum. Meas.*, vol. 65, no. 7, pp. 1547–1557, Jul. 2016.

[10] G. Jang, J. Kim, S. Lee, and Y. Choi, "EMG-based continuous control scheme with simple classifier for electric-powered wheelchair," *IEEE Trans. Ind. Electron.*, vol. 63, no. 6, pp. 3695–3705, Jun. 2016.

[11] V. D. A. Rocha, J. C. D. Carmo, and F. A. D. O. Nascimento, "Weighted-cumulated S-EMG muscle fatigue estimator," *IEEE J. Biomed. Health Inform.*, vol. 22, no. 6, pp. 1854–1862, Nov. 2018.

[12] D. Rubin and J. Daube, *Clinical Neurophysiology*, vol. 74, no. 6, 3rd ed. 2010, p. 529.

[13] G. T. Allison, P. Godfrey, and G. Robinson, "EMG signal amplitude assessment during abdominal bracing and hollowing," *J. Electromyogr. Kinesiol.*, vol. 8, no. 1, pp. 51–57, Feb. 1998.

[14] L.-Q. Zhang, R. Shiavi, M. A. Hunt, and J.-J.-J. Chen, "Clustering analysis and pattern discrimination of EMG linear envelopes," *IEEE Trans. Biomed. Eng.*, vol. 38, no. 8, pp. 777–784, Aug. 1991.

[15] H. Xie and Z. Wang, "Mean frequency derived via Hilbert-Huang transform with application to fatigue EMG signal analysis," *Comput. Methods Programs Biomed.*, vol. 82, no. 2, pp. 114–120, May 2006.

[16] P. Kutílek, J. Hýbl, J. Mareš, V. Socha, and P. Smrčka, "A myoelectric prosthetic arm controlled by a sensor-actuator loop," *Acta Polytechnica*, vol. 54, no. 3, pp. 197–204, Jun. 2014.

[17] L. Chen and Y. Hao, "Feature extraction and classification of EHG between pregnancy and labour group using Hilbert-Huang transform and extreme learning machine," *Comput. Math. Methods Med.*, vol. 2017, pp. 1–9, Feb. 2017.

[18] R. F. M. Kleissen and G. Zilvold, "Estimation uncertainty in ensemble averaged surface EMG profiles during gait," *J. Electromyogr. Kinesiol.*, vol. 4, no. 2, pp. 83–94, Jan. 1994.

[19] I. Stirn, T. J. Tomaz, V. P. Kapus, and V. Strojnik, "Evaluation of mean power spectral frequency of EMG signal during 100 metre crawl," *Europ. J. Sport Sci.*, vol. 13, no. 2, pp. 1–10, 2011.

[20] C. H. Yeh, H. W. V. Young, C. Y. Wang, Y. H. Wang, P. L. Lee, J. H. Kang, and M. T. Lo, "Quantifying spasticity with limited swinging cycles using pendulum test based on phase amplitude coupling," *IEEE Trans. Neural Syst. Rehabil. Eng.*, vol. 24, no. 10, pp. 1081–1088, Oct. 2016.

[21] R. M. Studer, R. J. P. D. Figueiredo, and G. S. Moschytz, "An algorithm for sequential signal estimation and system identification for EMG signals," *IEEE Trans. Biomed. Eng.*, vol. BME-31, no. 3, pp. 285–295, Mar. 1984.

[22] Y. Zhan, S. Guo, K. M. Kendrick, and J. Feng, "Filtering noise for synchronised activity in multi-trial electrophysiology data using Wiener and Kalman filters," *Biosystems*, vol. 96, no. 1, pp. 1–13, Apr. 2009.

[23] N. M. Lopez, F. D. Sciascio, C. M. Soria, and M. E. Valentinuzzi, "Robust EMG sensing system based on data fusion for myoelectric control of a robotic arm," *Biomed. Eng. OnLine*, vol. 8, no. 5, pp. 1–13, 2009.
[24] C. S. L. Tsui, J. Q. Gan, and S. J. Roberts, "A self-paced brain–computer interface for controlling a robot simulator: An online event labelling paradigm and an extended Kalman filter based algorithm for online training," *Med. Biol. Eng. Comput.*, vol. 47, no. 3, pp. 257–265, Mar. 2009.
[25] L. L. Menegaldo, "Real-time muscle state estimation from EMG signals during isometric contractions using Kalman filters," *Biol. Cybern.*, vol. 111, nos. 5–6, pp. 335–346, Dec. 2017.
[26] T. Triwiyanto, O. Wahyunggoro, H. A. Nugroho, and H. Herianto, "Muscle fatigue compensation of the electromyography signal for elbow joint angle estimation using adaptive feature," *Comput. Electr. Eng.*, vol. 71, pp. 284–293, Oct. 2018.
[27] D. Simon, *Optimal State Estimaiton: Kalman, H_∞, and Nonlinear Approaches*. Hoboken, NJ, USA: Wiley, 2006.
[28] K. J. Uribe-Murcia, Y. S. Shmaliy, C. K. Ahn, and S. Zhao, "Unbiased FIR filtering for time-stamped discretely delayed and missing data," *IEEE Trans. Autom. Control*, vol. 65, no. 5, pp. 2155–2162, May 2020.
[29] Y. S. Shmaliy, F. Lehmann, S. Zhao, and C. K. Ahn, "Comparing robustness of the Kalman, H_∞, and UFIR filters," *IEEE Trans. Signal Process.*, vol. 66, no. 13, pp. 3447–3458, Jul. 2018.
[30] S. Marquez-Figueroa, Y. S. Shmaliy, and O. Ibarra-Manzano, "Optimal extraction of EMG signal envelope and artifacts removal assuming colored measurement noise," *Biomed. Signal Process. Contr.*, vol. 57, Mar. 2020, Art. no. 101679.
[31] A. Bryson and L. Henrikson, "Estimation using sampled data containing sequentially correlated noise," *J. Spacecraft Rockets*, vol. 5, no. 6, pp. 662–665, 1968.
[32] M. G. Petovello, K. O'Keefe, G. Lachapelle, and M. E. Cannon, "Consideration of time-correlated errors in a Kalman filter applicable to GNSS," *J. Geodesy*, vol. 83, no. 1, pp. 51–53, 2009.
[33] Y. S. Shmaliy, S. Zhao, and C. K. Ahn, "Kalman and UFIR state estimation with coloured measurement noise using backward Euler method," *IET Signal Process.*, vol. 14, no. 2, pp. 64–71, Apr. 2020.
[34] N. Jiang, H. Rehbaum, I. Vujaklija, B. Graimann, and D. Farina, "Intuitive, online, simultaneous, and proportional myoelectric control over two degrees-of-freedom in upper limb amputees," *IEEE Trans. Neural Syst. Rehabil. Eng.*, vol. 22, no. 3, pp. 501–510, May 2014.
[35] G. Li, O. W. Samuel, C. Lin, M. G. Asogbon, P. Fang, and P. O. Idowu, "Realizing efficient EMG-based prosthetic control strategy," in *Neural Interface: Frontiers and Applications* (Advances in Experimental Medicine and Biology), X. Zheng, Ed. Singapore: Springer, 2019, ch. 6, pp. 149–166.
[36] Y. Shmaliy, S. Zhao, and C. K. Ahn, "Unbiased FIR filtering: An iterative alternative to Kalman filtering ignoring noise and initial conditions," *IEEE Contr. Syst. Mag.*, vol. 37, no. 5, pp. 70–89, Oct. 2017.
[37] Y. S. Shmaliy, "Unbiased FIR filtering of discrete-time polynomial state-space models," *IEEE Trans. Signal Process.*, vol. 57, no. 4, pp. 1241–1249, Apr. 2009.
[38] Y. S. Shmaliy, "An iterative Kalman-like algorithm ignoring noise and initial conditions," *IEEE Trans. Signal Process.*, vol. 59, no. 6, pp. 2465–2473, Jun. 2011.
[39] O. Aviles, J. Rodriguez, M. Herrera, and G. Martinez, "UCI machine learning repository," Iniversidad Militar Nueva Granada, Tecno Parque SENA nodo Manizales, Bogotá, Colombia, Tech. Rep. 52-48, 2012.
[40] M. Atzori, A. Gijsberts, C. Castellini, B. Caputo, A.-G.-M. Hager, S. Elsig, G. Giatsidis, F. Bassetto, and H. Müller, "Electromyography data for non-invasive naturally-controlled robotic hand prostheses," *Sci. Data*, vol. 1, no. 1, pp. 1–13, Dec. 2014.
[41] M. Atzori, A. Gijsberts, S. Heynen, A.-G. Mittaz Hager, O. Deriaz, P. van der Smagt, C. Castellini, B. Caputo, and H. Müller, "Building the Ninapro database: A resource for the biorobotics community," in *Proc. IEEE Int. Conf. Biomed. Robot. Biomechatron. (BioRob)*, Jun. 2012, pp. 1258–1265.
[42] M. Atzori, A. Gijsberts, I. Kuzborskij, S. Elsig, A.-G. M. Hager, O. Deriaz, C. Castellini, H. Müller, and B. Caputo, "Characterization of a benchmark database for myoelectric movement classification," *IEEE Trans. Neural Syst. Rehabil. Eng.*, vol. 23, no. 1, pp. 73–83, Jan. 2015.
[43] D. Simon and Y. S. Shmaliy, "Unified forms for Kalman and finite impulse response filtering and smoothing," *Automatica*, vol. 49, no. 6, pp. 1892–1899, Jun. 2013.
[44] L. J. Myers, M. Lowery, M. O'Malley, C. L. Vaughan, C. Heneghan, A. S. C. Gibson, Y. X. R. Harley, and R. Sreenivasan, "Rectification and non-linear pre-processing of EMG signals for cortico-muscular analysis," *J. Neurosci. Methods*, vol. 124, no. 2, pp. 157–165, Apr. 2003.
[45] J.-J.-J. Chen, R. G. Shiavi, and L.-Q. Zhang, "A quantitative and qualitative description of electromyographic linear envelopes for synergy analysis," *IEEE Trans. Biomed. Eng.*, vol. 39, no. 1, pp. 9–18, Jan. 1992.
[46] I. T. Young, L. J. van Vliet, and M. van Ginkel, "Recursive Gabor filtering," *IEEE Trans. Signal Process.*, vol. 50, no. 11, pp. 2798–2805, Nov. 2002.
[47] Y. Du, H. Wang, S. Qiu, W. Yao, P. Xie, and X. Chen, "An advanced adaptive control of lower limb rehabilitation robot," *Frontiers Robot. AI*, vol. 5, pp. 1–11, Oct. 2018.
[48] T. O'Halloran, M. Haugland, G. M. Lyons, and T. Sinkjaer, "An investigation of the effect of modifying stimulation profile shape on the loading response phase of gait, during FES-corrected drop foot: Stimulation profile and loading response," *Neuromodulation, Technol. Neural Interface*, vol. 7, no. 2, pp. 113–125, Apr. 2004.

SANDRA MARQUEZ-FIGUEROA (Member, IEEE) received the Engineering degree in communications and electronics from the Autonomous University of Zacatecas, Jalpa, México, in 2012, and the M.S. degree in electrical engineering from the Universidad de Guanajuato, Salamanca, Mexico, in 2015. She is currently pursuing the Ph.D. degree with the Universidad de Guanajuato, Mexico. Her research interests include bioengineering and biomedical signal processing.

YURIY S. SHMALIY (Fellow, IEEE) received the B.S., M.S., and Ph.D. degrees from Kharkiv Aviation Institute, Ukraine, in 1974, 1976, and 1982, respectively, all in electrical engineering, and the D.Sc. degree from the USSR Government, in 1992.

He serves as a Full Professor beginning in 1986. From 1985 to 1999, he was with Kharkiv Military University. In 1992, he founded the Scientific Center "Sichron," where he was the Director in 2002. Since 1999, he has been with Universidad de Guanajuato, Salamanca, Mexico, where he is also the Head of the Department of Electronics Engineering from 2012 to 2015. From 2015 to 2019, he was a Visiting Professor with City University London, London, U.K., and TELECOM SudParis, Evry, France. He has published 483 journal and conference papers and holds 81 patents. He has also published the books *Continuous-Time Signals* (Springer, 2006) and *Continuous-Time Systems* (Springer, 2007), *GPS-Based Optimal FIR Filtering of Clock Models* (New York: Nova Science Publishers, 2009), and edited book *Probability: Interpretation, Theory and Applications* (New York: Nova Science Publishers, 2012). His discrete orthogonal polynomials are called Discrete Shmaliy Moments. His current interests include optimal and robust state estimation. He was awarded the title Honorary Radio Engineer of the USSR, in 1991. He received the Royal Academy of Engineering Newton Research Collaboration Program Award in 2015, the IEEE Latin America Eminent Engineer Award in 2021, and several conference Best Paper Awards. He was invited many times to give tutorials, seminars, and plenary lectures.

OSCAR G. IBARRA-MANZANO (Member, IEEE) was born in Mexico, in 1968. He received the B.S. degree in communications and electronics and the M.E. degree in electrical engineering degrees from the University of Guanajuato, Salamanca, in 1990 and 1993, respectively, and the Ph.D. degree in electrical engineering from the National Institute for Astrophysics Optics and Electronics, Puebla, Mexico, in 1999. In January 1991, he joined the University of Guanajuato. He has been a full-time Professor and the Chair of the Electronics Engineering Department, since 2000. From December 2003 to September 2012, he served as the Dean for the Mechanical, Electrical and Electronics Engineering School.